Su-Li Cheng,[1] Abraham Behrmann,[1] Jian-Su Shao,[2] Bindu Ramachandran,[1] Karen Krchma,[1] Yoanna Bello Arredondo,[1] Attila Kovacs,[3] Megan Mead,[1] Robert Maxson,[4] and Dwight A. Towler[1,5]

Targeted Reduction of Vascular *Msx1* and *Msx2* Mitigates Arteriosclerotic Calcification and Aortic Stiffness in *LDLR*-Deficient Mice Fed Diabetogenic Diets

Diabetes 2014;63:4326–4337 | DOI: 10.2337/db14-0326

COMPLICATIONS

When fed high-fat diets, male *LDLR*$^{-/-}$ mice develop obesity, hyperlipidemia, hyperglycemia, and arteriosclerotic calcification. An osteogenic *Msx-Wnt* regulatory program is concomitantly upregulated in the vasculature. To better understand the mechanisms of diabetic arteriosclerosis, we generated *SM22-Cre;Msx1(fl/fl);Msx2(fl/fl);LDLR*$^{-/-}$ mice, assessing the impact of *Msx1+Msx2* gene deletion in vascular myofibroblast and smooth muscle cells. Aortic *Msx2* and *Msx1* were decreased by 95% and 34% in *SM22-Cre;Msx1(fl/fl);Msx2(fl/fl);LDLR*$^{-/-}$ animals versus *Msx1(fl/fl);Msx2(fl/fl);LDLR*$^{-/-}$ controls, respectively. Aortic calcium was reduced by 31%, and pulse wave velocity, an index of stiffness, was decreased in *SM22-Cre;Msx1(fl/fl);Msx2(fl/fl);LDLR*$^{-/-}$ mice vs. controls. Fasting blood glucose and lipids did not differ, yet *SM22-Cre;Msx1(fl/fl);Msx2(fl/fl);LDLR*$^{-/-}$ siblings became more obese. Aortic adventitial myofibroblasts from *SM22-Cre;Msx1(fl/fl);Msx2(fl/fl);LDLR*$^{-/-}$ mice exhibited reduced osteogenic gene expression and mineralizing potential with concomitant reduction in multiple *Wnt* genes. Sonic hedgehog (*Shh*) and *Sca1*, markers of aortic osteogenic progenitors, were also reduced, paralleling a 78% reduction in alkaline phosphatase (TNAP)–positive adventitial myofibroblasts. RNA interference revealed that although *Msx1+Msx2* supports *TNAP* and *Wnt7b* expression, *Msx1* selectively maintains *Shh* and *Msx2* sustains *Wnt2, Wnt5a, and Sca1* expression in aortic adventitial myofibroblast cultures. Thus, *Msx1* and *Msx2* support vascular mineralization by directing the osteogenic programming of aortic progenitors in diabetic arteriosclerosis.

Vascular calcification increasingly afflicts the aging population, driven by the dysmetabolic milieus of diabetes, dyslipidemia, and uremia (1–4). In type 2 diabetes, arterial vascular calcification primarily occurs within the tunica media, with contributions from atherosclerotic plaques as they accrue. Both medial and atherosclerotic calcification increase vascular stiffness, thus impairing Windkessel physiology, the elasticity of conduit vessels that enables smooth distal tissue perfusion throughout the cardiac cycle (3,5). During systole, compliant conduit vessels capture kinetic energy as potential energy then release this energy during diastole as a mechanism that sustains perfusion pressure with cardiac relaxation (5). When conduit vessels lose elasticity, cardiac afterload and myocardial oxygen consumption are increased, tissue perfusion becomes increasingly pulsatile in distal vascular beds, and risks for end-organ barotrauma and ischemia are increased during systole and

[1]Sanford-Burnham Medical Research Institute, Orlando, FL
[2]MD Anderson Cancer Center, Houston, TX
[3]Washington University in St. Louis, St. Louis, MO
[4]Norris Cancer Center, University of Southern California, Los Angeles, CA
[5]Translational Research Institute for Metabolism and Diabetes, Florida Hospital, Orlando, FL

Corresponding author: Dwight A. Towler, dtowler@sanfordburnham.org.

Received 24 February 2014 and accepted 9 July 2014.

This article contains Supplementary Data online at http://diabetes.diabetesjournals.org/lookup/suppl/doi:10.2337/db14-0326/-/DC1.

See accompanying article, p. 4011.

diastole, respectively (5). The net consequence is increased cardiovascular morbidity and mortality through stroke, myocardial infarction, congestive heart failure, and lower-extremity amputation (1,2).

When fed high-fat diets, male LDLR$^{-/-}$ mice develop obesity, hyperlipidemia, insulin-resistant diabetes, and arterial calcification (6–9). These responses phenocopy the arteriosclerotic pathobiology observed in patients with diabetes (1). *Msx1* and *Msx2* are homeodomain transcription factors indispensible for craniofacial bone formation (10) and cardiac valve morphogenesis (11,12), and the osteogenic *Msx* gene regulatory program is concomitantly upregulated in calcifying arteries of diabetic mice and humans with diabetes, dyslipidemia, and/or uremia-induced vascular disease (1,2,13). Thus, mineralization programs regulated by *Msx* genes are activated during vascular calcium accrual in the setting of type 2 diabetes.

In previous studies, we demonstrated that augmenting aortic *Msx2* gene expression through either tumor necrosis factor–dependent proinflammatory signals or direct *Msx2* transgenic strategies worsens arterial calcification (8,9,14). We addressed whether reducing aortic *Msx* gene expression mitigates arteriosclerotic calcification to provide additional proof for the role of this gene regulatory pathway in arterial disease biology. Implementing Cre-lox technology and the *SM22-Cre* transgenic mouse (15), we show that targeted reductions in vascular smooth muscle *Msx2* and *Msx1* (10,16,17) reduce arterial calcification and improve arterial compliance in diabetic *LDLR*$^{-/-}$ mice, with concomitant reductions in the mineralizing potential of vascular osteoprogenitors.

RESEARCH DESIGN AND METHODS

Cell Culture Reagents, Biochemicals, Antibodies, and Immunohistochemistry

Molecular, biochemical, genotyping, and histological methods have been previously detailed (7–9,18). The indicated, inventoried TaqMan Gene Expression assays were purchased from Life Technologies for quantifying mRNA accumulation by real-time fluorescence quantitative RT-PCR (qRT-PCR). Genotyping primers were ordered from Life Technologies. Amplimer pairs were as follows: SM22-Cre, 5′-CAG ACA CCG AAG CTA CTC TCC TTC C-3′ and 5′-CGC ATA ACC AGT GAA ACA GCA TTG C-3′ (500 bp); Msx1, 5′-ACA CTA TGC TTG ATG TGG TCC CAG GCG-3′ and 5′-GGG CTC GGC CAA TCA AAT TAG AGA G-3′ (wild type [WT] = 165 bp; flox = 233 bp); Msx2, 5′-GTT TCA TGA CCT CAT TAC TCA CGC TG-3′ and 5′-GGT ACC TTT GTC AAA TCT GTG AG-3′ (WT = 158 bp; flox = 226 bp); and LDLR$^{-/-}$, 5′-ACC CCA AGA CGT GCT CCC AGG ATG-3′ and 5′-CGC AGT GCT CCT CAT CTG ACT TGT C-3′ for the genomic site of insertion (intact WT = 383 bp) and 5′-AGG ATC TCG TCG TGA CCC ATG GCG A-3′ and 5′-GAG CGG CGA TAC CGT AAA GCA CGA GG-3′ for neomycin (200 bp). ELISA kits quantifying matrix metabolism markers desmosine (CSB-E14196M; American Research Products) and type I collagen propeptide P1NP (AC-33F1; IDS Inc.) were purchased from commercial sources. Lipofectamine RNAiMAX, ON-TARGETplus control and SMARTpool small interfering RNAs (siRNAs) targeting *Msx1* and *Msx2* were purchased from Life Technologies. GSK3β/phospho-GSK3β antibodies were from Cell Signaling Technologies (8,9,14).

Generation and Evaluation of *SM22-Cre;Msx1(fl/fl);Msx2(fl/fl);LDLR*$^{-/-}$ Mice

Procedures for handling mice were approved by the Washington University and Sanford-Burnham institutional animal care and use committees. *LDLR*$^{-/-}$*B6.129S7-Ldlrtm1Her/J* (19) and *SM22-CreTg(Tagln-cre)1Her/J* (15) mice were obtained from The Jackson Laboratory. *Msx1(fl/fl);Msx2(fl/fl)* mice have been described (20) and were bred onto the *LDLR*$^{-/-}$ background. Experimental *SM22-Cre;Msx1(fl/fl);Msx2(fl/fl);LDLR*$^{-/-}$, *SM22-Cre;Msx2(fl/fl);LDLR*$^{-/-}$, and *Msx1(fl/fl);Msx2(fl/fl);LDLR*$^{-/-}$ control animals were obtained through the breeding scheme outlined in Fig. 1. At 5–10 weeks of age, animals were weighed. Male sibling cohorts (n = 4–13 per genotype as indicated) of *Msx1(fl/fl);Msx2(fl/fl);LDLR*$^{-/-}$ and *SM22-Cre;Msx1(fl/fl);Msx2(fl/fl);LDLR*$^{-/-}$ mice with equivalent starting weights were challenged with high-fat western diet (HFD) (TD88137; Teklad Lab Animal Diets; Harlan) for 2 months. At the end of the dietary challenge, thoracic aortas were harvested, weighed, and extracted for calcium, collagen, or total RNA, implementing methods previously detailed (9,21).

Assessment of Aortic Stiffness by Aortic Pulse Wave Velocity

Cohorts of male *Msx1(fl/fl);Msx2(fl/fl);LDLR*$^{-/-}$ and *SM22-Cre;Msx1(fl/fl);Msx2(fl/fl);LDLR*$^{-/-}$ mice were challenged with HFD for 3 months. Aortic arch pulse wave velocity (PWV) was determined as described (21) using a modification of the transit time method (22), implementing a Vevo 770 ultrasound system with a 30-MHz transducer (VisualSonics Inc., Toronto, ON, Canada). Under isofluorane anesthesia, the ascending aorta, aortic arch, and proximal portion of the descending aorta were imaged in one two-dimensional imaging plane from the right-side superior parasternal view. The pulse wave Doppler sample volume was placed first near the aortic valve to record blood flow velocity in the proximal aorta then promptly moved to the visualized portion of the descending aorta without changing the imaging plane to record blood flow velocity in the descending aorta. The curvilinear distance between the proximal and distal points of the aortic velocity interrogation (D2–D1 in millimeters) was measured using the exact coordinates of the Doppler sample volumes. The time delay between the onset of flow velocity in the distal and proximal portions of the aorta (T2–T1 in milliseconds) was measured relative to the simultaneously recorded electrocardiogram signal. PWV was calculated as the ratio of D2–D1 to T2–T1 expressed as meters per second.

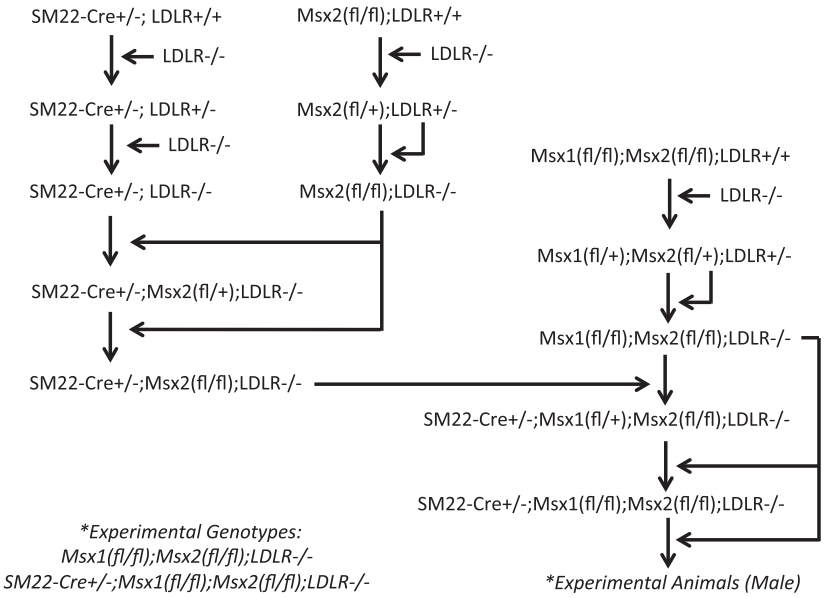

Figure 1—Flow diagram of breeding strategy implemented to generate experimental *SM22-Cre;Msx1(fl/fl);Msx2(fl/fl);LDLR*$^{-/-}$ mice and *Msx1(fl/fl);Msx2(fl/fl);LDLR*$^{-/-}$ controls. *Msx1(fl/fl);Msx2(fl/fl)* (20), *LDLR*$^{-/-}$ (19), and *SM22-Cre* (15) transgenic mice on the C57BL/6 background were generated as described and then bred as indicated to generate male sibling cohorts for subsequent dietary challenge and characterization. See RESEARCH DESIGN AND METHODS for the specific PCR amplimers used for genotyping.

Preparation of Primary Aortic Adventitial Mesenchymal Cell Cultures

Aortic adventitial myofibroblasts were prepared using a modification of published methods (14,23). Aortas were isolated from *Msx1(fl/fl);Msx2(fl/fl);LDLR*$^{-/-}$ and *SM22-Cre;Msx1(fl/fl);Msx2(fl/fl);LDLR*$^{-/-}$ mice by dissection from diaphragm to aortic outflow and processed, and cell isolates were pooled (8–10 male mice per genotype). After rinsing twice in PBS supplemented with penicillin-streptomycin-fungizone (PSF) 200 Units/mL, 200 μg/mL, 2.5 μg/mL with intervening blotting on Kimwipes to remove blood, each aorta was rinsed three times in fresh DMEM supplemented with PSF. Individual aortas were then minced into four fragments. Two aortas per genotype were placed in a 50-mL conical screw cap tube and then digested at 37°C in a 5% CO_2 incubator in 4 mL of type I collagenase 1 mg/mL (catalog number LS004149; Worthington Biochemical Corporation), DNase I 60 Units/mL (D5025; Sigma-Aldrich), and hyaluronidase 0.5 mg/mL (H3506; Sigma-Aldrich) in DMEM with PSF using a sterile flea stir bar to provide gentle agitation. Two sequential 1-h digestions were performed and combined, and cells were pelleted at 1,500 rpm for 5 min. The cell pellet was resuspended in DMEM with 10% FBS supplemented with PSF and then plated onto 10-cm tissue culture plates coated with rat tail type I collagen 6 μg/cm^2. After 3 days, one-half of the medium was removed from each culture and replaced with fresh growth medium. Two days later, cells were rinsed once with growth medium lacking PSF and then maintained in growth media with penicillin-streptomycin 100 International Units/mL, 100 μg/mL and fed every 3 days until confluence. Only passage 1 and passage 2 cultures were used for experimentation. The methods for preparation of SFG-LacZ and SFG-Wnt7b retroviruses and myofibroblast transduction have been described (18). RNA interference (RNAi) in primary adventitial cultures was performed in 12-well cluster dishes (100,000 cells/well) in triplicate with 100 nmol/L nontargeting control siRNA (NTC), 50 nmol/L *Msx1* siRNA + 50 nmol/L NTC, 50 nmol/L *Msx2* siRNA + 50 nmol/L NTC, or 50 nmol/L *Msx1* + 50 nmol/L *Msx2* siRNA using RNAiMAX, following the manufacturer's protocol. Two days later, RNA was isolated for qRT-PCR using previously detailed methods (18).

Alkaline Phosphatase Staining of Aortic Primary Cell Cultures

Alkaline phosphatase–positive cells in aortic adventitial cell cultures were visualized as previously described, but using the Vector Red fluorescent substrate (14,18). Briefly, aortic mesenchymal cells were cultured on a type I collagen–precoated four-chamber slide (60,000 cells/chamber) for 8 days. During the final 6 days, cells were treated with β-glycerophosphate 5 mmol/L and ascorbic acid 50 μg/mL. Cells were then washed three times with Tris-buffered saline (TBS) (20 mmol/L Tris HCl, 1.5 mol/L NaCl, pH 7.5), fixed with 4% paraformaldehyde in TBS for 4 min, and rinsed three times with TBS. Staining with Vector Red reagent (Vector Red Alkaline Phosphatase Substrate Kit I, catalog number SK-5100; Vector Laboratories) was performed for 1 h in the dark per the manufacturer's protocol. After washing three times with TBS and twice with distilled water, nuclei were stained with DAPI (Prolong Gold Antifade Reagent,

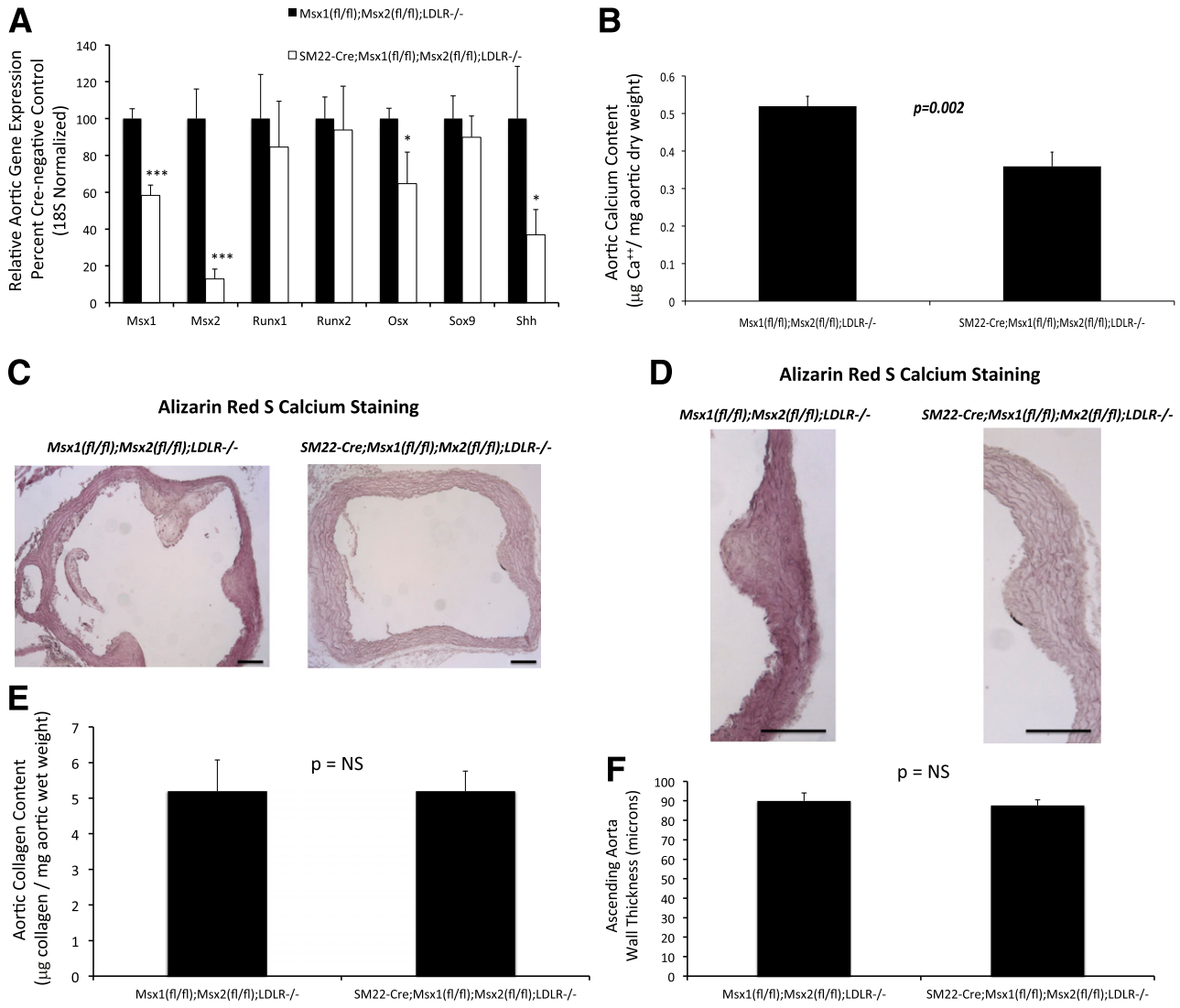

Figure 2—Conditional deletion of *Msx1* and *Msx2* in the VSMC lineage reduces arteriosclerotic calcification in *LDLR*$^{-/-}$ mice fed diabetogenic HFDs. *A*: qRT-PCR of aortic RNA verified Cre-dependent reductions in aortic *Msx1* and *Msx2* gene expression in *SM22-Cre;Msx1(fl/fl);Msx2(fl/fl);LDLR*$^{-/-}$ mice. Although *Runx* genes were not affected, *Shh*, a marker of the adventitial osteoprogenitor, and the osteogenic zinc finger transcription factor *Osx* were significantly reduced (n = 4–5 per genotype). *B*: Biochemical measurement of aortic calcium content following acidic extraction revealed significantly reduced aortic calcification in *SM22-Cre;Msx1(fl/fl);Msx2(fl/fl);LDLR*$^{-/-}$ mice (n = 9–13 per genotype). *C*: Alizarin Red S staining revealed calcification within the tunica media. *D*: Higher power magnification of aortic wall in *C*. Scale bars = 100 μm. *E*: No differences were noted in aortic collagen content (n = 7–8 per genotype). *F*: Histomorphometric wall thickness was also not affected by vascular *Msx* deficiency (n = 3 per genotype). *$P < 0.05$, ***$P < 0.001$. NS, not significant.

catalog number P36931; Molecular Probes) and the slides coverslipped. Photomicrographs of alkaline phosphatase–positive fluorescent cells (TX2 filter cube), nuclei (DAPI filter cube), and phase contrast images were captured by a Leica DM4000 B fluorescence microscope at ×200 magnification.

Calcium Staining of Aortic Primary Cell Cultures

Aortic adventitial cells were seeded in type I collagen–coated 24-well cluster plates (15,000 cells/well, three wells per genotype). The next day and every other day thereafter, cells were fed with DMEM containing 10% FBS, ascorbic acid 50 μg/mL, and β-glycerophosphate 5 mmol/L for a total of 12 days. Mineralized matrix was detected by Alizarin Red S staining as described (14,18), and images (12–16 images/well) were captured by a Nikon Eclipse Ti microscope at ×100 magnification. Alizarin red–stained areas were quantified using National Institutes of Health ImageJ software as previously detailed (14).

Statistics

All experiments were performed with 3–12 independent replicates per group. Statistical analyses were performed using GraphPad InStat version 3.06 software, implementing standard parametric or nonparametric methods

(two-tailed testing) when indicated. Graphic data are presented as mean ± SEM.

RESULTS

Reductions in Aortic *Msx1* and *Msx2* mitigate Arteriosclerotic Calcification Responses in *LDLR*-Deficient Mice Fed High-Fat Diabetogenic Diets

Msx1 and *Msx2* are highly related members of the NK-like homeodomain transcription factor family (11,12). *Msx1* and *Msx2* play quantitatively distinct, but functionally redundant roles in neural crest biology, craniofacial and heart valve morphogenesis, and skeletal and ectodermal organ growth at sites where dynamic epithelial-mesenchymal interactions occur (11,12). Our previous studies demonstrated that an HFD upregulates *Msx1* and *Msx2* in the aortic myofibroblasts and smooth muscle cells in male $LDLR^{-/-}$ mice (6,23), presaging subsequent cardiovascular calcification and the expression of several osteogenic Wnt ligands, including *Wnt3*, *Wnt5*, and *Wnt7* family members (7). Moreover, transgenic augmentation of aortic *Msx2* expression promoted calcification in the tunica media in mice fed HFD, with mineralization proceeding through activation of an osteogenic Wnt cascade (7). To better understand the role of endogenous *Msx1* and *Msx2* in vascular disease processes, including arteriosclerotic calcification, we implemented Cre-Lox technology to reduce aortic *Msx1* and *Msx2* tone in genetically engineered mice possessing floxed (fl) *Msx* alleles (20). The *SM22-Cre* transgene was used to deliver Cre recombinase to vascular smooth muscle cells (VSMCs) and aortic myofibroblasts (15). Using the breeding scheme outlined in Fig. 1, *SM22-Cre;Msx1(fl/fl);Msx2(fl/fl);LDLR*$^{-/-}$ and *Msx1(fl/fl);Msx2(fl/fl);LDLR*$^{-/-}$ mice were generated and male sibling cohorts studied. *Msx1* and *Msx2* mRNAs were significantly reduced in total aortic RNA from *SM22-Cre;Msx1(fl/fl);Msx2(fl/fl);LDLR*$^{-/-}$ mice versus *Msx1(fl/fl);Msx2(fl/fl);LDLR*$^{-/-}$ controls, with concomitant reductions in osterix (*Osx*), a zinc finger transcription factor upregulated by *Msx2* (23,24) and necessary for osteogenic mineralization (25) (Fig. 2*A*). Although the abundance of *Runx1*, *Runx2*, and *Sox9* messages were unaltered in total aortic RNA, expression of Sonic hedgehog (*Shh*), a marker of the vascular multipotent mesenchymal progenitor (26), was concomitantly reduced with vascular *Msx* gene deficiency. We next challenged sibling male cohorts with the diabetogenic HFD for 2 months and assessed the impact

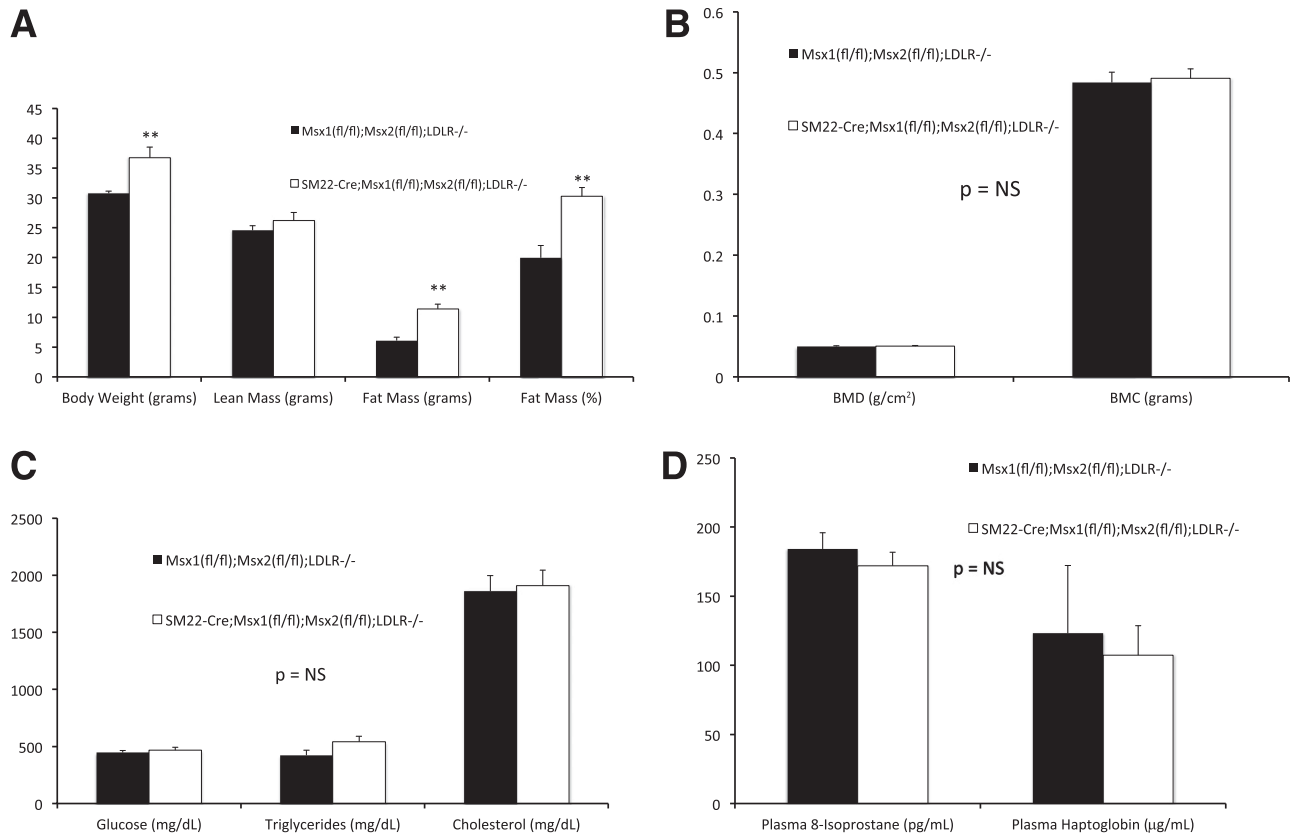

Figure 3—Conditional deletion of *Msx1* and *Msx2* in the VSMC lineage augments fat mass but does not alter bone mass or diet-induced changes in fasting glucose or lipid profiles in $LDLR^{-/-}$ mice. *A*: Body weight and composition assessed by DEXA revealed increased body fat in *SM22-Cre;Msx1(fl/fl);Msx2(fl/fl);LDLR*$^{-/-}$ mice vs. *Msx1(fl/fl);Msx2(fl/fl);LDLR*$^{-/-}$ controls when fed an HFD for 2 months. *B*: No difference in bone mineral content or areal density was observed. *C*: Fasting glucose, triglyceride, and cholesterol levels were unaltered. *D*: Fasting plasma 8-isoprostane and haptoglobin levels were also unaltered (n = 9–13 per genotype). $^{**}P < 0.01$. BMC, bone mineral content; BMD, bone mineral density; NS, not significant.

on aortic calcium accumulation. Compared with *Msx1(fl/fl);Msx2(fl/fl);LDLR*$^{-/-}$ controls, *SM22-Cre;Msx1(fl/fl);Msx2(fl/fl);LDLR*$^{-/-}$ mice exhibited a significant 31% reduction in total aortic calcium accrual (Fig. 2*B*). Alizarin red staining for aortic calcium confirmed that changes in mineral deposition largely localized within the tunica media (Fig. 2*C* and *D*). By contrast, total aortic collagen accumulation (Fig. 2*E*) and ascending aorta wall thickness (Fig. 2*F*) were unaltered. *SM22-Cre;Msx1(fl/fl);Msx2(fl/fl);LDLR*$^{-/-}$ mice were significantly more obese than *Msx1(fl/fl);Msx2(fl/fl);LDLR*$^{-/-}$ controls (Fig. 3*A*), but bone mineral density and bone mineral content by DEXA were also unaltered (Fig. 3*B*). No significant differences were observed with respect to diet-induced changes in fasting plasma glucose, triglyceride, or cholesterol levels (Fig. 3*C*). Furthermore, plasma haptoglobin and 8-F-isoprostanes, markers of systemic inflammation and oxidative stress upregulated by diabetogenic HFD (8), did not differ with vascular *Msx* gene deletion (Fig. 3*D*), indicating that genetic manipulation of vascular *Msx* genes had not mitigated the proinflammatory metabolic milieu. Thus, aortic *Msx1* and *Msx2* expression in aortic VSMCs and myofibroblasts supports arteriosclerotic calcification in LDLR$^{-/-}$ mice fed a diabetogenic HFD.

Reductions in Aortic *Msx1* and *Msx2* Reduce Arteriosclerotic Vascular Stiffening

Arterial calcification is a harbinger of vascular stiffness, a composite of material properties and geometric properties that alter the distensibility of conduit vessels during the cardiac cycle (3). From the Moens-Korteweg relationship (27), the product of the elastic modulus and the arterial wall thickness-to-lumen diameter ratio is proportional to the square of the conduit vessel PWV; thus, PWV is an index of vessel stiffness arising from contributions of vessel material properties (e.g., calcification, fibrosis) and geometric properties (wall thickness, diameter) (3). We therefore assessed aortic arch PWV in *SM22-Cre;Msx1(fl/fl);Msx2(fl/fl);LDLR*$^{-/-}$ mice and *Msx1(fl/fl);Msx2(fl/fl);LDLR*$^{-/-}$ controls after 3 months of HFD, implementing Doppler echocardiography as a noninvasive and clinically useful method to assess aortic stiffness (22). As shown in Fig. 4*A*, aortic arch PWV was significantly reduced by 30% in *SM22-Cre;Msx1(fl/fl);Msx2(fl/fl);LDLR*$^{-/-}$ mice ($P < 0.05$ vs. controls), indicating reduced vascular stiffness. Importantly, aortic diameters did not differ between Cre-minus and Cre-plus cohorts at the ascending aorta (1.3 ± 0.05 vs. 1.4 ± 0.05 mm), aortic arch (1.1 ± 0.05 vs. 1.2 ± 0.03 mm), or descending aorta (0.9 ± 0.02 vs. 1.0 ± 0.04 mm; all *P* not significant) (Fig. 4*B*). Plasma markers of matrix remodeling and synthesis, namely the elastin degradation product desmosine (28) and type I procollagen N-telopeptide (9), did not significantly differ between *Msx1(fl/fl);Msx2(fl/fl);LDLR*$^{-/-}$ and *SM22-Cre;Msx1(fl/fl);Msx2(fl/fl);LDLR*$^{-/-}$ animals (Supplementary Fig. 1). Thus, reducing arterial *Msx1* and *Msx2* expression mitigates vascular stiffness in a murine model of diet-induced diabetic arteriosclerosis. Reductions in vascular calcification, but not changes in vascular diameter, wall thickness, or fibrosis, accompany reductions in vascular stiffness.

Osteogenic Gene Regulatory Programs and *Wnt* Gene Expression Are Reduced in Aortic Myofibroblasts Isolated From *SM22-Cre;Msx1(fl/fl);Msx2(fl/fl);LDLR*$^{-/-}$ Mice

Reductions in arteriosclerotic calcification and vascular stiffness with reduced *Shh* expression suggested that key components of vascular mesenchymal progenitor differentiation were perturbed in aortic myofibroblasts from *SM22-Cre;Msx1(fl/fl);Msx2(fl/fl);LDLR*$^{-/-}$ mice. Therefore, we studied expression of transcriptional markers of early osteogenic, adipogenic, chondrogenic, and myogenic differentiation in aortic adventitial myofibroblasts stimulated with a dexamethasone cocktail used to enhance mesenchymal cell differentiation from progenitors

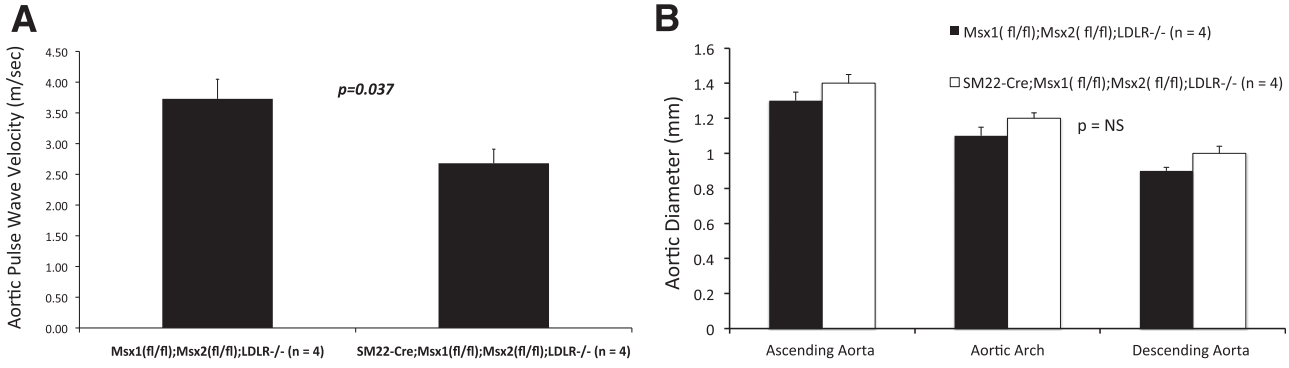

Figure 4—Aortic PWV, a measure of arterial stiffness, is reduced in *SM22-Cre;Msx1(fl/fl);Msx2(fl/fl);LDLR*$^{-/-}$ mice. Male *Msx1(fl/fl);Msx2(fl/fl);LDLR*$^{-/-}$ mice and *SM22-Cre;Msx1(fl/fl);Msx2(fl/fl);LDLR*$^{-/-}$ male sibling cohorts were challenged with HFD for 3 months then evaluated by Doppler echocardiography to quantify aortic stiffness as previously described using PWV. *A*: Compared with *Msx1(fl/fl);Msx2(fl/fl);LDLR*$^{-/-}$ controls, *SM22-Cre;Msx1(fl/fl);Msx2(fl/fl);LDLR*$^{-/-}$ mice exhibited significantly reduced aortic arch PWV (n = 4 per genotype). *B*: Aortic diameters did not differ between genotypes as assessed by echocardiography. Recall that although calcification was decreased, no change in aortic wall thickness or collagen content was observed (Fig. 2). See RESULTS for discussion. NS, not significant.

(29). As shown in Fig. 5*A*, primary aortic myofibroblasts generated from male *SM22-Cre;Msx1(fl/fl);Msx2(fl/fl);LDLR*$^{-/-}$ mice exhibit deficiencies in *Dlx5*, *PPARG*, *Sox9*, and myocardin (*Myocd*) gene expression with concomitant Cre-dependent reductions in *Msx1*, and *Msx2*. An impact at an early stage of osteogenic differentiation is likely because levels of *BSP* (bone sialoprotein) and *OCN* (osteocalcin), the latter a gene of mature osteoblasts directly inhibited by Msx2 (30), were both reduced in *SM22-Cre;Msx1(fl/fl);Msx2(fl/fl);LDLR*$^{-/-}$ cultures (Fig. 5*B*). Consistent with this notion, *Shh* and *Sca1*, markers of adventitial osteoprogenitors (26), were concomitantly diminished with combined *Msx1+Msx2* deficiency (Fig. 5*B*). Expression of leptin and *OPN* (osteopontin) were unaffected (Fig. 5*B*).

Increasing *Msx2* tone in adventitial myofibroblasts by either viral transduction or transgene expression upregulates

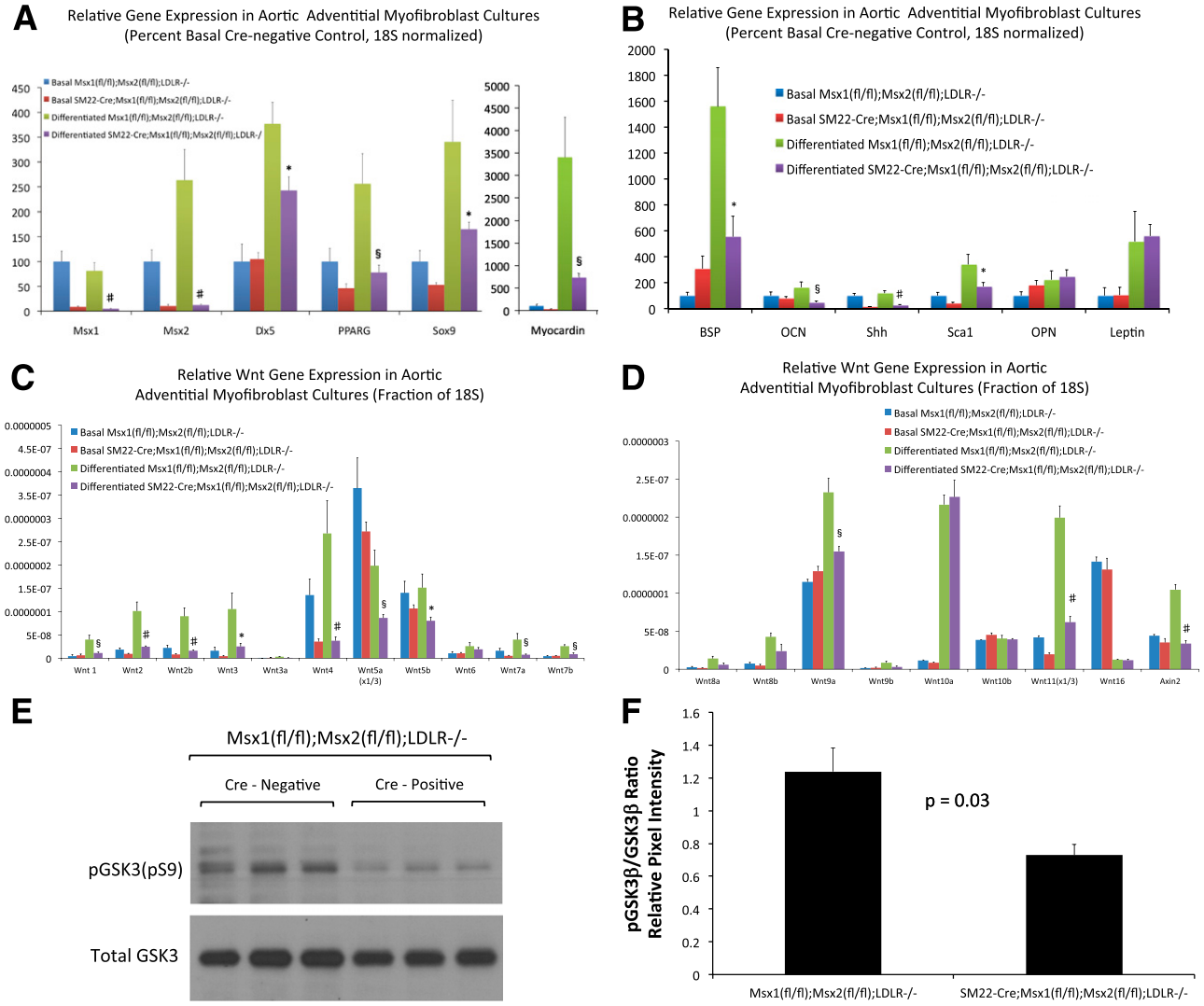

Figure 5—Primary aortic myofibroblasts from *SM22-Cre;Msx1(fl/fl);Msx2(fl/fl);LDLR*$^{-/-}$ mice exhibit reductions in differentiation-induced expression of early osteochondrogenic, adipogenic, and myogenic transcriptional regulators with concomitant deficiency in multiple Wnt gene programs. Primary aortic adventitial myofibroblasts were isolated then induced to undergo differentiation, implementing a modification of a dexamethasone-based protocol used to drive mesenchymal differentiation (29). RNA was extracted for qRT-PCR for the gene indicated (18S normalized). *A*: Note that increases in early osteogenic (*Msx1*, *Msx2*, *Dlx5*) (47,48), osteochondrogenic (*Sox9*) (35), adipogenic (*PPARG*) (49), and smooth muscle myogenic (50) (*Myocd*) transcriptional regulators were reduced in *SM22-Cre;Msx1(fl/fl);Msx2(fl/fl);LDLR*$^{-/-}$ myofibroblasts vs. *Msx1(fl/fl);Msx2(fl/fl);LDLR*$^{-/-}$ controls. *B*: *Shh* and *Sca1*, markers of the early multipotent adventitial progenitor (26), were also reduced in *Msx*-deficient myofibroblasts. Concomitant reductions in osteoblast-specific differentiation markers (*BSP*, *OCN*) were noted, whereas *OPN* and leptin were unaffected. *C* and *D*: The expression of multiple Wnt ligands, including those previously demonstrated to be upregulated by *Msx2* overexpression (7), was reduced in *SM22-Cre;Msx1(fl/fl);Msx2(fl/fl);LDLR*$^{-/-}$ myofibroblasts. The expression levels of Wnt5a and Wnt11, the two most abundant transcripts, have been scaled by a factor of one-third as indicated to facilitate presentation of all transcripts. The Wnt/β-catenin target gene *Axin2* was simultaneously downregulated, whereas *Wnt10a* and *Wnt10b* were unaffected by *Msx* deficiency. *E* and *F*: Ser-9 phospho-GSK3β, an independent index of activated Wnt signaling, was also significantly reduced in *SM22-Cre;Msx1(fl/fl);Msx2(fl/fl);LDLR*$^{-/-}$ myofibroblasts as revealed by Western blot. *$P < 0.05$, §$P < 0.01$, #$P < 0.001$ vs. differentiated Cre-negative control.

a cohort of genes encoding *Wnt* ligands (7). Therefore, we examined the impact of *Msx1+Msx2* deficiency on the expression of all 19 Wnt ligands. As shown in Fig. 5*C* and *D*, the relative expression of *Wnt1*, *Wnt2*, *Wnt2b*, *Wnt3*, *Wnt4*, *Wnt5a*, *Wnt5b*, *Wnt7a*, *Wnt7b*, *Wnt8b*, *Wnt9a*, and *Wnt11* was reduced by ≥50% in *SM22-Cre;Msx1(fl/fl);Msx2(fl/fl);LDLR*$^{-/-}$ cultures. *Wnt10a* and *Wnt10b* were unaffected. *Axin2*, a genomic target entrained to canonical Wnt/β-catenin signaling in multiple cell types (31), was also downregulated (Fig. 5*D*). GSK3β phosphorylation, another index of activated *Wnt* signaling (32), was concomitantly reduced in *SM22-Cre;Msx1(fl/fl);Msx2(fl/fl);LDLR*$^{-/-}$ cultures as well (Fig. 5*E* and *F*). Thus, combined *Msx1* and *Msx2* deficiency in *SM22-Cre;Msx1(fl/fl);Msx2(fl/fl);LDLR*$^{-/-}$ aortic myofibroblasts reduces elaboration of differentiated mesenchymal cell transcripts, including the expression of osteogenic and *Wnt* gene regulatory programs.

Alkaline Phosphatase–Positive and Alizarin Red–Positive Osteogenic Nodules Are Reduced in Aortic Myofibroblasts Isolated From *SM22-Cre;Msx1(fl/fl);Msx2(fl/fl);LDLR*$^{-/-}$ Mice

We and others previously demonstrated that aortic adventitial myofibroblasts and calcifying vascular cells residing within the tunica media exhibit osteogenic, myogenic, and limited adipogenic potential when cultured (23,26,33). Moreover, transduction with a retrovirus driving expression of *Msx2* promotes osteogenesis in aortic myofibroblasts (23). However, the consequences of depleting endogenous *Msx* signaling upon vascular mesenchymal osteogenic differentiation are unknown. Therefore, we prepared primary aortic myofibroblasts from male *SM22-Cre;Msx1(fl/fl);Msx2(fl/fl);LDLR*$^{-/-}$ and *Msx1(fl/fl);Msx2(fl/fl);LDLR*$^{-/-}$ sibling controls, cultured them under mineralizing conditions, and quantified alkaline phosphatase and mineralizing Alizarin red osteogenic colonies as previously described (14,23). As shown in Fig. 6*A* and *B*, the numbers of alkaline phosphatase–positive adventitial myofibroblasts decreased by 78% in aortas of *Msx*-deficient mice compared with controls. Moreover, through Alizarin red staining quantifying calcified colonies, mineralization was shown to be concomitantly decreased by 43% (Fig. 6*C* and *D*). Reduced calcification was partly due to diminished *Wnt* gene bioactivity because transduction of *SM22-Cre;Msx1(fl/fl);Msx2(fl/fl);LDLR*$^{-/-}$ cells with a retrovirus driving *Wnt7b* expression restored Alizarin red staining (Supplementary Fig. 2). Thus, the

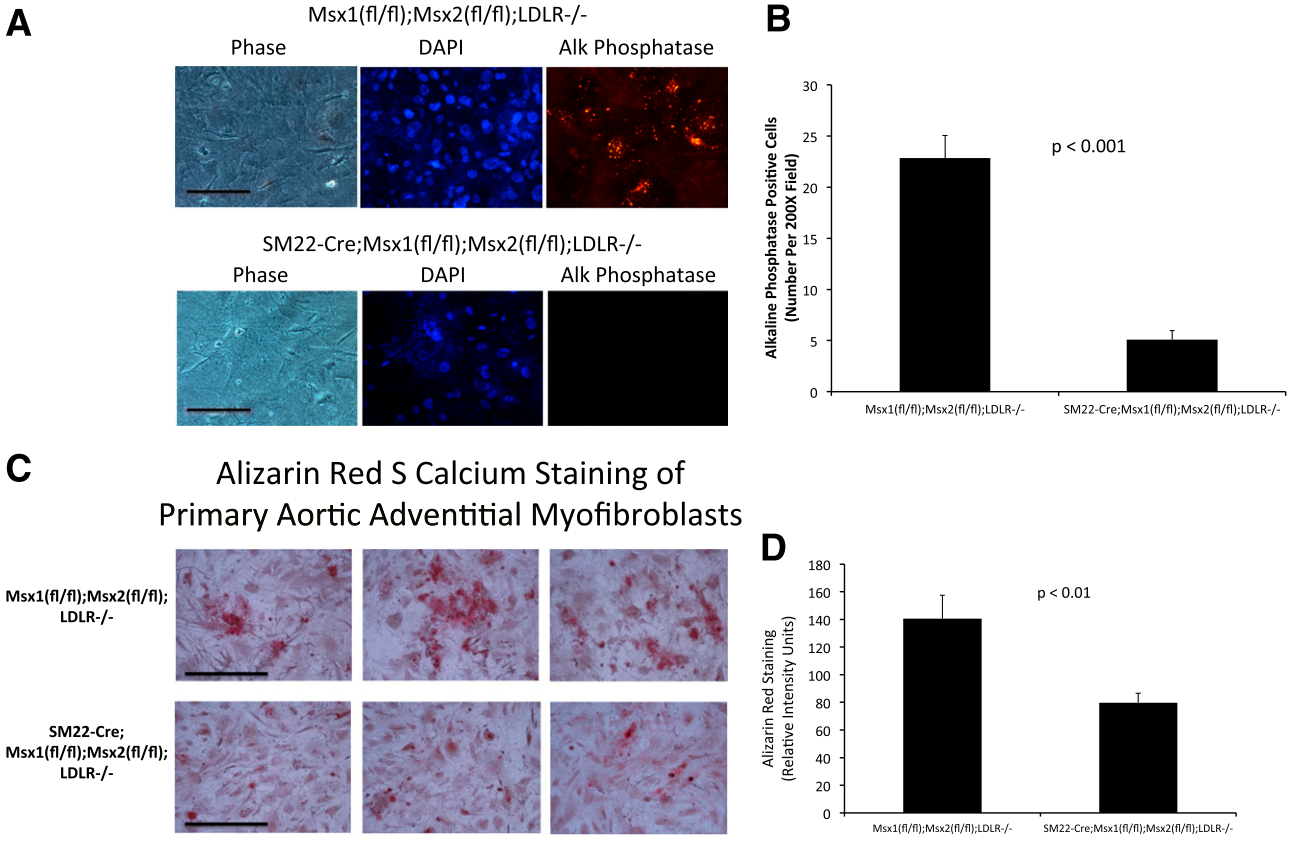

Figure 6—Primary aortic myofibroblasts from *SM22-Cre;Msx1(fl/fl);Msx2(fl/fl);LDLR*$^{-/-}$ mice exhibit reductions in alkaline phosphatase–positive osteoprogenitors and Alizarin Red S calcium staining. Primary aortic adventitial myofibroblasts were isolated from male *SM22-Cre;Msx1(fl/fl);Msx2(fl/fl);LDLR*$^{-/-}$ mice and male *Msx1(fl/fl);Msx2(fl/fl);LDLR*$^{-/-}$ controls, cultured under osteogenic conditions, and then analyzed for alkaline phosphatase cell numbers and calcium deposition by Alizarin Red S staining as previously described (14). Alkaline phosphatase–positive cell numbers were reduced in *SM22-Cre;Msx1(fl/fl);Msx2(fl/fl);LDLR*$^{-/-}$ mice (*A* and *B*) (n = 31–33 fields per genotype in two independent cultures) as was Alizarin red staining (*C* and *D*). Scale bar = 25 μm. Alk, alkaline.

combined *Msx1* and *Msx2* deficiency in *SM22-Cre;Msx1(fl/fl);Msx2(fl/fl);LDLR*$^{-/-}$ aortas reduces the osteogenic mineralization potential of vascular myofibroblasts.

Msx1 and *Msx2* Play Overlapping, Yet Distinct Roles in Support of Osteogenic Programs Elaborated by Aortic Adventitial Myofibroblasts

In a separate experimental cohort, conditional deletion of the *Msx2* gene alone was insufficient to reduce aortic calcium accumulation in response to an HFD challenge (1.2 ± 0.2 vs. 1.1 ± 0.2 μg calcium/g aorta in *Msx2(fl/fl);LDLR*$^{-/-}$ and *SM22-Cre;Msx2(fl/fl);LDLR*$^{-/-}$ mice, respectively; n = 9–11 per genotype; P not significant), indicating some functional redundancy. To better understand the individual contributions of *Msx1* and *Msx2* to adventitial myofibroblast biology, we implemented RNAi to reduce *Msx1*, *Msx2*, or *Msx1+Msx2* expression in primary cell cultures, quantifying the impact on osteogenic lineage programming, *TNAP* (34), and cardiogenic (32) *Wnt* (*Wnt2*, *Wnt5a*, *Wnt7b*, *Wnt11*) gene expression. As shown in Fig. 7*A*, RNAi selectively and specifically reduced *Msx* gene expression in transfected aortic adventitial myofibroblast cultures. *TNAP* and *Wnt7b* messages were downregulated by siRNA targeting either *Msx1* or *Msx2*. By contrast, *Wnt5a* and *Wnt2* expression were downregulated primarily in response to *Msx2* depletion. Unlike cultures from *SM22-Cre;Msx1(fl/fl);Msx2(fl/fl);LDLR*$^{-/-}$ mice, *Wnt11* expression was not acutely altered by RNAi targeting *Msx1+Msx2*. Passman et al. (26) previously identified an *Shh*-, *Sca1*-, and *Msx1*-expressing multipotent adventitial cell population capable of osteogenic differentiation. We therefore assessed the impact of *Msx1* and *Msx2* RNAi on expression of these specific adventitial progenitor markers, further encompassing *CD90+CD105* as general markers of mesenchymal stem cell populations (26), and *Sox9* as a marker of the osteochondroprogenitor (35). As shown in Fig. 7*B*, siRNA targeting *Msx1* selectively reduced *Shh* expression. By contrast, siRNA targeting *Msx2* preferentially downregulated *Sca1* and *Sox9*, whereas *CD90* and *CD105* were unaffected. Thus, *Msx1* and *Msx2* program aortic adventitial osteoprogenitors through overlapping, yet distinct mechanisms that control *Wnt* and *Shh* gene expression.

DISCUSSION

Msx1 and *Msx2* play fundamental roles in signaling cascades controlling craniofacial morphogenesis and epithelial-mesenchymal interactions driving odontogenesis, cardiac cushion formation, and breast development (10–12). *Msx2* is also upregulated in aortic valve and vascular myofibroblasts during the progression of diet-induced diabetes in preclinical models of vascular calcification (6,7). Atherogenic stimuli such as tumor necrosis factor, interleukin-1β, and lipid products derived from oxidized LDL all upregulate *Msx2* in vascular mesenchymal cells (8,14,36). Furthermore, transgenic overexpression of *Msx2* in the vessel wall promotes vascular calcification and activation of Wnt-dependent osteogenic gene regulatory programs (7). Importantly, *Msx2* is elaborated in sclerotic vessel (1,2) and valve (13) segments in humans with arteriosclerosis. However, the contributions of endogenous *Msx* genes to cardiovascular disease during postnatal life, including vascular calcification, have not been previously examined. Because of the functionally redundant roles of *Msx1* and *Msx2* in vital developmental processes (10–12,17), we addressed the impact of combined *Msx1* and *Msx2* vascular deficiency on arteriosclerotic disease in *LDLR*$^{-/-}$ mice.

Consistent with the current results demonstrating the activation of aortic osteogenic mineralization in transgenic mice overexpressing *Msx2* (7), reductions in vascular *Msx* tone elicit reciprocal changes; aortic calcium accrual is reduced alongside reductions in vascular stiffness in *SM22-Cre;Msx1(fl/fl);Msx2(fl/fl);LDLR*$^{-/-}$ mice versus *Msx1(fl/fl);Msx2(fl/fl);LDLR*$^{-/-}$ controls. Reductions in aortic calcification and stiffness occurred in the absence of significant improvements in metabolic status. Aortic collagen

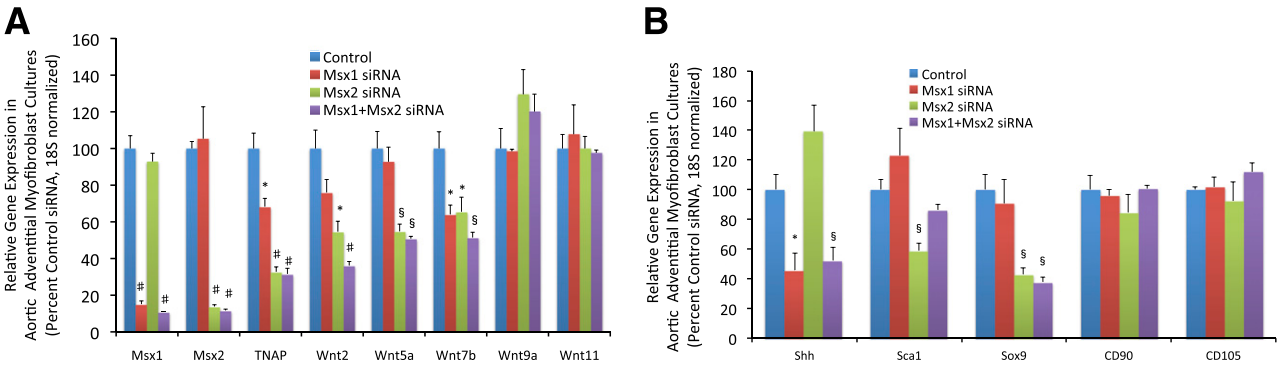

Figure 7—*Msx1* and *Msx2* program aortic adventitial osteoprogenitors through overlapping, yet distinct mechanisms that control *Wnt* and *Shh* gene expression. Primary aortic adventitial cells were transfected with either a control nontargeting siRNA or an siRNA targeting *Msx1* or *Msx2* as indicated. RNA was extracted 2 days later, and gene expression analyzed by qRT-PCR. *A*: Note that although *Msx1* and *Msx2* both support *TNAP* and *Wnt7b* expression, *Wnt2* and *Wnt5a* depend on *Msx2*. *B*: The aortic adventitial progenitor markers *Shh* and *Sca1* differentially responded to *Msx* RNAi, with *Msx1* supporting *Shh* expression. *Sca1* and *Sox9* mRNAs were selectively downregulated by RNAi targeting *Msx2*. CD90 and CD105 were unaffected. See RESULTS for details. *P < 0.05, §P < 0.01, and #P < 0.001 vs. nontargeting siRNA control.

accumulation and vascular wall thickness, other contributors to vascular stiffness (3), were unaltered, suggesting a fundamental contribution of endogenous *Msx* gene tone to vascular calcium and osteoprogenitor homeostasis. Consistent with this notion, ex vivo analysis of vascular adventitial myofibroblasts from *SM22-Cre;Msx1(fl/fl);Msx2(fl/fl);LDLR*$^{-/-}$ mice revealed reductions in Alizarin red calcium staining and expression of bone-specific markers. Because *Msx1* and *Msx2* are cell-autonomous inhibitors of *OCN* gene transcription (6,30), but *OCN* mRNA levels were reduced with *Msx* deficiency, we considered the possibility that reductions in *Msx* tone might reduce osteoprogenitor numbers. This was confirmed by enumerating alkaline phosphatase–positive cells arising in the adventitial myofibroblast population. Passman et al. (26) first identified that *Shh* demarcates the renewable mesenchymal progenitors with osteogenic potential within the aorta. We therefore examined the impact of *Msx1+Msx2* deficiency on *Shh* expression and identified significant reductions in *Shh* in aortic myofibroblast cultures. Concomitant reductions in multiple *Wnt*s not only confirm our previous studies indicating that *Wnt* genes are entrained to *Msx* tone but also suggest that the Wnt ligand milieu may be critical to development and maintenance of osteoprogenitors. Canonical Wnt signals can also upregulate both *Msx1* and *Msx2* gene expression (37), introducing the notion of feed-forward regulation. Thus, endogenous *Msx* signaling contributes to vascular calcification, directing prosclerotic gene regulatory programs that drive osteoprogenitor development and differentiation (7,23,24).

RNAi confirmed the role of *Msx* genes in *TNAP* and *Wnt* expression. Paracrine Wnt signals are important for the elaboration of osteogenic *TNAP* expression downstream of BMP2 and Shh (38). Of note, although commonalities exist in *Msx1* and *Msx2* regulation of *TNAP* and *Wnt7b*, *Msx1* appears to play a uniquely important role in support of *Shh* expression. By contrast, *Msx2* is more important in the elaboration of *Wnt5a* and *Wnt2*. Taken together, these data suggest that *Msx1* and *Msx2* differentially support *Shh* and *Wnt* signaling pathways to promote the osteogenic programming of adventitial progenitors. Future studies will identify genomic complexes targeted by Msx1 versus Msx2.

Of note, global *Msx1+Msx2* deficiency results in embryonic lethality and abnormal cardiac morphogenesis due to cardiac neural crest hyperproliferation (12). Additionally, hypoplastic myocardial atrioventricular cushions in *Msx1*$^{-/-}$;*Msx2*$^{-/-}$ embryos arise from impaired endothelial-mesenchymal transitioning necessary for atrioventricular valve formation (11). Thus, the cardiac defects of *Msx1*$^{-/-}$; *Msx2*$^{-/-}$ embryos relate to aberrant tissue remodeling and hemodynamics arising from perturbed endothelial-mesenchymal transitioning and cell type–specific proliferative control (11,12). We speculate that the cardiovascular developmental consequences of *Msx* deficiency may be more significant in the endothelial lineage than in the VSMC lineage.

There are limitations to our studies. The current data newly establish the role for endogenous vascular *Msx* genes in diabetic arteriosclerosis, vessel stiffness, and the osteogenic potential of vascular myofibroblasts and confirm the impact of *Msx1+Msx2* on *Wnt* gene expression. However, the specific Wnt ligands programmed by *Msx1+Msx2* as necessary for osteoprogenitor development and differentiation have yet to be characterized. Multiple noncanonical as well as canonical Wnt ligands are regulated. *Wnt11*, *Wnt5a*, and *Wnt7b* are capable of provoking both noncanonical and canonical signals, depending on context (39), and these ligands participate in both osteogenesis and fibrogenesis (9,40,41). Other important *Wnt*s are also expressed by aortic myofibroblasts (42,43), and the increased body fat observed in *SM22-Cre;Msx1(fl/fl);Msx2(fl/fl);LDLR*$^{-/-}$ mice following HFD challenge likely arises in part due to reduced *Wnt* tone (44). Finally, *Msx1+Msx2* deficiency did not completely eliminate vascular calcium accrual. As Speer et al. (45) and Byon et al. (46) have shown, a Runx2-positive cell population is responsible for ~80% of the vascular osteogenic cells within the vessel wall, driving osteogenic mineralization in response to oxidative stress. *Msx1+Msx2* deficiency did not abrogate vascular *Runx2* expression, and we speculate that *Runx2* osteogenic programming contributes to residual disease. Nevertheless, the current data demonstrate that significant reductions in vascular calcification, with concomitant reductions in arterial stiffness, can be achieved through reductions in arterial *Msx* signaling. Future studies will identify the specific Wnt ligands required for programming osteogenic differentiation and vascular calcification in conjunction with *Msx1+Msx2*. Targeted inhibition of these ligands and their cognate receptors may phenocopy, in part, the beneficial actions of myofibroblast *Msx* deficiency in arteriosclerotic disease and thus offer a therapeutic strategy.

Funding. This work was supported by National Institutes of Health grants HL-69229 and HL-81138 to D.A.T. and DE-016320 to R.M., the Barnes-Jewish Hospital Foundation, and the Sanford-Burnham Medical Research Institute.

Duality of Interest. D.A.T. serves as a consultant for Eli Lilly, Daiichi-Sankyo, and Merck & Co. No other potential conflicts of interest relevant to this article were reported.

Author Contributions. S.-L.C., A.B., J.-S.S., and A.K. researched data and reviewed and edited the manuscript. B.R., K.K., Y.B.A., and M.M. researched data. R.M. reviewed and edited the manuscript. D.A.T. researched data and wrote the manuscript. D.A.T. is the guarantor of this work and, as such, had full access to all the data in the study and takes responsibility for the integrity of the data and the accuracy of the data analysis.

References

1. Tyson KL, Reynolds JL, McNair R, Zhang Q, Weissberg PL, Shanahan CM. Osteo/chondrocytic transcription factors and their target genes exhibit distinct patterns of expression in human arterial calcification. Arterioscler Thromb Vasc Biol 2003;23:489–494

2. Koleganova N, Piecha G, Ritz E, et al. Arterial calcification in patients with chronic kidney disease. Nephrol Dial Transplant 2009;24:2488–2496

3. Greenwald SE. Ageing of the conduit arteries. J Pathol 2007;211: 157–172

4. Boström KI, Rajamannan NM, Towler DA. The regulation of valvular and vascular sclerosis by osteogenic morphogens. Circ Res 2011;109:564–577
5. Safar ME, Boudier HS. Vascular development, pulse pressure, and the mechanisms of hypertension. Hypertension 2005;46:205–209
6. Towler DA, Bidder M, Latifi T, Coleman T, Semenkovich CF. Diet-induced diabetes activates an osteogenic gene regulatory program in the aortas of low density lipoprotein receptor-deficient mice. J Biol Chem 1998;273:30427–30434
7. Shao JS, Cheng SL, Pingsterhaus JM, Charlton-Kachigian N, Loewy AP, Towler DA. Msx2 promotes cardiovascular calcification by activating paracrine Wnt signals. J Clin Invest 2005;115:1210–1220
8. Al-Aly Z, Shao JS, Lai CF, et al. Aortic Msx2-Wnt calcification cascade is regulated by TNF-alpha-dependent signals in diabetic Ldlr-/- mice. Arterioscler Thromb Vasc Biol 2007;27:2589–2596
9. Cheng SL, Shao JS, Halstead LR, Distelhorst K, Sierra O, Towler DA. Activation of vascular smooth muscle parathyroid hormone receptor inhibits Wnt/beta-catenin signaling and aortic fibrosis in diabetic arteriosclerosis. Circ Res 2010;107:271–282
10. Satokata I, Ma L, Ohshima H, et al. Msx2 deficiency in mice causes pleiotropic defects in bone growth and ectodermal organ formation. Nat Genet 2000;24:391–395
11. Chen YH, Ishii M, Sucov HM, Maxson RE Jr. Msx1 and Msx2 are required for endothelial-mesenchymal transformation of the atrioventricular cushions and patterning of the atrioventricular myocardium. BMC Dev Biol 2008;8:75
12. Chen YH, Ishii M, Sun J, Sucov HM, Maxson RE Jr. Msx1 and Msx2 regulate survival of secondary heart field precursors and post-migratory proliferation of cardiac neural crest in the outflow tract. Dev Biol 2007;308:421–437
13. Miller JD, Chu Y, Brooks RM, Richenbacher WE, Peña-Silva R, Heistad DD. Dysregulation of antioxidant mechanisms contributes to increased oxidative stress in calcific aortic valvular stenosis in humans. J Am Coll Cardiol 2008;52:843–850
14. Lai CF, Shao JS, Behrmann A, Krchma K, Cheng SL, Towler DA. TNFR1-activated reactive oxidative species signals up-regulate osteogenic Msx2 programs in aortic myofibroblasts. Endocrinology 2012;153:3897–3910
15. Boucher P, Gotthardt M, Li WP, Anderson RG, Herz J. LRP: role in vascular wall integrity and protection from atherosclerosis. Science 2003;300:329–332
16. Ishii M, Han J, Yen HY, Sucov HM, Chai Y, Maxson RE Jr. Combined deficiencies of Msx1 and Msx2 cause impaired patterning and survival of the cranial neural crest. Development 2005;132:4937–4950
17. Han J, Ishii M, Bringas P Jr, Maas RL, Maxson RE Jr, Chai Y. Concerted action of Msx1 and Msx2 in regulating cranial neural crest cell differentiation during frontal bone development. Mech Dev 2007;124:729–745
18. Cheng SL, Shao JS, Behrmann A, Krchma K, Towler DA. Dkk1 and MSX2-Wnt7b signaling reciprocally regulate the endothelial-mesenchymal transition in aortic endothelial cells. Arterioscler Thromb Vasc Biol 2013;33:1679–1689
19. Ishibashi S, Brown MS, Goldstein JL, Gerard RD, Hammer RE, Herz J. Hypercholesterolemia in low density lipoprotein receptor knockout mice and its reversal by adenovirus-mediated gene delivery. J Clin Invest 1993;92:883–893
20. Fu H, Ishii M, Gu Y, Maxson R. Conditional alleles of Msx1 and Msx2. Genesis 2007;45:477–481
21. Shao JS, Sierra OL, Cohen R, et al. Vascular calcification and aortic fibrosis: a bifunctional role for osteopontin in diabetic arteriosclerosis. Arterioscler Thromb Vasc Biol 2011;31:1821–1833
22. Hartley CJ, Taffet GE, Michael LH, Pham TT, Entman ML. Noninvasive determination of pulse-wave velocity in mice. Am J Physiol 1997;273:H494–H500
23. Cheng SL, Shao JS, Charlton-Kachigian N, Loewy AP, Towler DA. MSX2 promotes osteogenesis and suppresses adipogenic differentiation of multipotent mesenchymal progenitors. J Biol Chem 2003;278:45969–45977
24. Cheng SL, Shao JS, Cai J, Sierra OL, Towler DA. Msx2 exerts bone anabolism via canonical Wnt signaling. J Biol Chem 2008;283:20505–20522
25. Koga T, Matsui Y, Asagiri M, et al. NFAT and Osterix cooperatively regulate bone formation. Nat Med 2005;11:880–885
26. Passman JN, Dong XR, Wu SP, et al. A sonic hedgehog signaling domain in the arterial adventitia supports resident Sca1+ smooth muscle progenitor cells. Proc Natl Acad Sci U S A 2008;105:9349–9354
27. Marque V, Kieffer P, Gayraud B, Lartaud-Idjouadiene I, Ramirez F, Atkinson J. Aortic wall mechanics and composition in a transgenic mouse model of Marfan syndrome. Arterioscler Thromb Vasc Biol 2001;21:1184–1189
28. Umeda H, Aikawa M, Libby P. Liberation of desmosine and isodesmosine as amino acids from insoluble elastin by elastolytic proteases. Biochem Biophys Res Commun 2011;411:281–286
29. Grigoriadis AE, Heersche JN, Aubin JE. Differentiation of muscle, fat, cartilage, and bone from progenitor cells present in a bone-derived clonal cell population: effect of dexamethasone. J Cell Biol 1988;106:2139–2151
30. Willis DM, Loewy AP, Charlton-Kachigian N, Shao JS, Ornitz DM, Towler DA. Regulation of osteocalcin gene expression by a novel Ku antigen transcription factor complex. J Biol Chem 2002;277:37280–37291
31. Leung JY, Kolligs FT, Wu R, et al. Activation of AXIN2 expression by beta-catenin-T cell factor. A feedback repressor pathway regulating Wnt signaling. J Biol Chem 2002;277:21657–21665
32. Cohen ED, Tian Y, Morrisey EE. Wnt signaling: an essential regulator of cardiovascular differentiation, morphogenesis and progenitor self-renewal. Development 2008;135:789–798
33. Tintut Y, Alfonso Z, Saini T, et al. Multilineage potential of cells from the artery wall. Circulation 2003;108:2505–2510
34. Kiffer-Moreira T, Yadav MC, Zhu D, et al. Pharmacological inhibition of PHOSPHO1 suppresses vascular smooth muscle cell calcification. J Bone Miner Res 2013;28:81–91
35. Akiyama H, Kim JE, Nakashima K, et al. Osteo-chondroprogenitor cells are derived from Sox9 expressing precursors. Proc Natl Acad Sci U S A 2005;102:14665–14670
36. Taylor J, Butcher M, Zeadin M, Politano A, Shaughnessy SG. Oxidized low-density lipoprotein promotes osteoblast differentiation in primary cultures of vascular smooth muscle cells by up-regulating Osterix expression in an Msx2-dependent manner. J Cell Biochem 2011;112:581–588
37. Willert J, Epping M, Pollack JR, Brown PO, Nusse R. A transcriptional response to Wnt protein in human embryonic carcinoma cells. BMC Dev Biol 2002;2:8
38. Rawadi G, Vayssière B, Dunn F, Baron R, Roman-Roman S. BMP-2 controls alkaline phosphatase expression and osteoblast mineralization by a Wnt autocrine loop. J Bone Miner Res 2003;18:1842–1853
39. Cha SW, Tadjuidje E, White J, et al. Wnt11/5a complex formation caused by tyrosine sulfation increases canonical signaling activity. Curr Biol 2009;19:1573–1580
40. Tu X, Joeng KS, Nakayama KI, et al. Noncanonical Wnt signaling through G protein-linked PKCdelta activation promotes bone formation. Dev Cell 2007;12:113–127
41. Friedman MS, Oyserman SM, Hankenson KD. Wnt11 promotes osteoblast maturation and mineralization through R-spondin 2. J Biol Chem 2009;284:14117–14125
42. Alfieri CM, Cheek J, Chakraborty S, Yutzey KE. Wnt signaling in heart valve development and osteogenic gene induction. Dev Biol 2010;338:127–135
43. Tsaousi A, Williams H, Lyon CA, et al. Wnt4/β-catenin signaling induces VSMC proliferation and is associated with intimal thickening. Circ Res 2011;108:427–436
44. Kennell JA, MacDougald OA. Wnt signaling inhibits adipogenesis through beta-catenin-dependent and -independent mechanisms. J Biol Chem 2005;280:24004–24010
45. Speer MY, Yang HY, Brabb T, et al. Smooth muscle cells give rise to osteochondrogenic precursors and chondrocytes in calcifying arteries. Circ Res 2009;104:733–741
46. Byon CH, Javed A, Dai Q, et al. Oxidative stress induces vascular calcification through modulation of the osteogenic transcription factor Runx2 by AKT signaling. J Biol Chem 2008;283:15319–15327

47. Takai H, Mezawa M, Choe J, Nakayama Y, Ogata Y. Osteogenic transcription factors and proto-oncogene regulate bone sialoprotein gene transcription. J Oral Sci 2013;55:209–215
48. Hassan MQ, Javed A, Morasso MI, et al. Dlx3 transcriptional regulation of osteoblast differentiation: temporal recruitment of Msx2, Dlx3, and Dlx5 homeodomain proteins to chromatin of the osteocalcin gene. Mol Cell Biol 2004;24:9248–9261
49. Kang S, Bennett CN, Gerin I, Rapp LA, Hankenson KD, Macdougald OA. Wnt signaling stimulates osteoblastogenesis of mesenchymal precursors by suppressing CCAAT/enhancer-binding protein alpha and peroxisome proliferator-activated receptor gamma. J Biol Chem 2007;282:14515–14524
50. Wang Z, Wang DZ, Pipes GC, Olson EN. Myocardin is a master regulator of smooth muscle gene expression. Proc Natl Acad Sci U S A 2003;100:7129–7134